Numerical simulation of the distortion in conventional laser and fluxless laser-plasma brazing of aluminum using Simufact.welding

P. Khazan, Hamburg/DE, T. Radel and P. Woizeschke, Bremen/DE

Brazing is a common technology for joining of aluminum components. Besides conventional methods, laser brazing is about to be established as a standard brazing technology. It offers several advantages compared to welding, e.g. less thermal induced stresses and less rework of the seam surface. A combination of conventional plasma and laser sources in a hybrid brazing process promises further improvements like the prevention of flux application. Numerical simulation of brazing processes, based on welding simulation software, offers the possibility to predict distortion and stress fields as well as material evolution due to work hardening effects.
In this paper, conventional laser brazing with flux usage and fluxless laser-plasma hybrid brazing are compared with respect to the distortion of bead-on-plate braze samples after additional postprocessing by cooling and cutting. Aluminum sheets of the alloy EN AW-6082 and the filler material EN AW-4047 are used. The feasibility of brazing simulation based on structural welding simulation approach is shown enabling the analysis and the prediction of the influences of process parameters and final machining in order to improve the process design and equipment configurations. The numerical simulations are validated by brazing experiments.

1 Introduction

Laser beam brazing is a well-established joining process for zinc-coated steel in the automotive industry [1]. Compared to steel, laser brazing of aluminum is less established as, for example, the removing of the naturally formed oxide layer is still challenging [2]. The conventional usage of fluxes [3] extends the process chain by the additional steps of application, drying, and post process removal of flux residues [4]. Furthermore, increased contamination of the system technology [5] and health risks [6] due to flux application are disadvantageous. Hence, fluxless processes are preferable. Adding a second process has been found as capable approach for removing the oxide layer, e.g. pulse laser [4] or arc processes [7]. Additionally, the brazing speed can be increased in case of laser-arc hybrid processes compared to single-arc variants due to the stabilization effect on the arc by the laser beam [8], particularly in leading configuration [9]. For industrial applications, a compact design of the laser-arc hybrid system technology is required [10]. Suitable hybrid-arc combinations are laser-TIG, laser-MIG and laser-plasma.
Structural welding simulation is a well-established tool for predicting distortions and stresses as well as material evolutions resulting from the welding process. Numerical analysis helps to improve the design of the joining process and, furthermore, the design of components and assemblies [11]. This structural approach does not target the investigation of process affecting factors like wetting or humping. However, structural welding simulation can calculate and predict the influences of transient or quasi-stationary heat sources, generated thermal strains and resulting stresses and deformations as well as, if applicable, metallurgical transformations. Thus, the number of needed experiments and, as a result, the costs for finding a suitable process design can be reduced. Overall, an increased understanding of the process and its parameter dependencies helps to improve the quality of the final product.

Modeling of laser and hybrid laser-plasma brazing processes is, in general, similar to the welding ones. Geometries of solidified braze seams have to be supplied as input data. In order to compare the solely laser with the hybrid laser-plasma process with regard to the resulting final shape of the brazed components, i.e. the distortion, the seam geometries are determined experimentally by metallographic cross-sections. Thus, macro-scale effects like the deformation of the joined components are considered by a structural simulation approach [12].
In this paper, we deal with two bead-on-plate brazing processes. While the solely laser process uses a flux agent, the hybrid laser-plasma process is fluxless.
Finite-Element-Method (FEM) is in principle well-suited for the prediction of distortions and stresses during brazing processes [11]. However, influences of flux usage can only be considered in terms of resulting seam geometries. Besides different final shapes of seams the two processes are based on different heat sources which is well considerable by a structural simulation. The build-up of the models as well as calculations has been carried out using the recent software release of Simufact.welding (5.0.1). The software Simufact.welding is well-suited for such studies because of powerful and easy-to-use GUI which supports definition of thermal loads, boundary conditions as well as material data management.

2 Experimental set-up for aluminum brazing

In the experiments, the laser beam is guided through a circular tungsten electrode resulting in a coaxial set-up, **Fig. 1**. An Nd:YAG rod laser source (Trumpf HL 4006D) is used. The optic contains a 56 mm collimation and a 280 mm focusing lens, respectively, which results in combination with a 600 µm fiber core diameter in a nominal focal diameter of 3 mm. The focal plane is set on the base material surface. Argon has been applied for the plasma process and as shielding gas. An EWM Tetrix 500 AC/DC power source has been used in DCEP (direct current electrode positive) configuration.

The specimens of the alloy EN AW-6082, heat treated in T6 standard, have the size of 150 x 50 x 2 mm³. The filler wire (EN AW-4047 Ø 1.2 mm) is oriented in leading configuration. Toggle clamps held the specimen from one side during brazing. The sheet surfaces were cleaned with ethanol before processing. In case of the solely laser process, additionally, flux (Fontargen F 400 NH) were applied. The type of joint is bead-on-plate.

Fig. 1. Coaxial set-up for fluxless hybrid laser-plasma brazing (BIAS ID 160081).

After the brazing process and a cool-down period, the specimens were unclamped. A 10 mm strip was extracted for cross-section measurements from each specimen, **Fig. 2**. The bending angles of the cut edges of both remaining parts (left and right) were measured by a tactile 3D coordinate measuring system to determine the typical angular distortion.

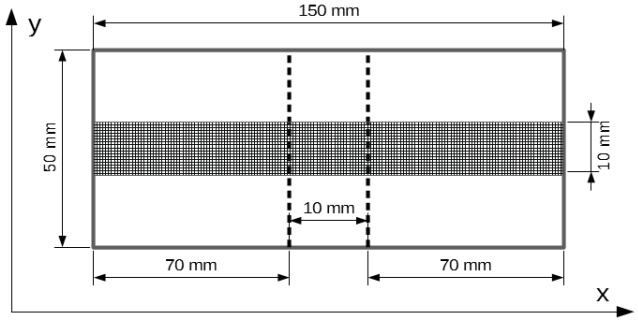

Fig. 2. Geometry specifics of the model according to the experiments (visible mesh refinement area in the middle section).

3 Experimental results

Cross-sections of brazed seams show longer wetting lengths, i.e. wider seams, in case of the hybrid laser-plasma process in comparison with the solely laser one, **Fig. 3**. Both cross-sections do not show any melting of the base material sheets.
The fluxless laser-plasma brazing process as well as the resulting brazing seam are shown, **Fig. 4**. The resulting seam shows a uniform appearance along the seam length, Next to the smooth seam, the typical cathodic cleaned surface is visible.
The bending angles of the specimens brazed by the hybrid laser-plasma and the solely laser process are determined to the averages of 1.13° ± 0.12° and 1.29° ± 0.17°, respectively. Thus, the measured distortion does not significantly differ between the two processes.

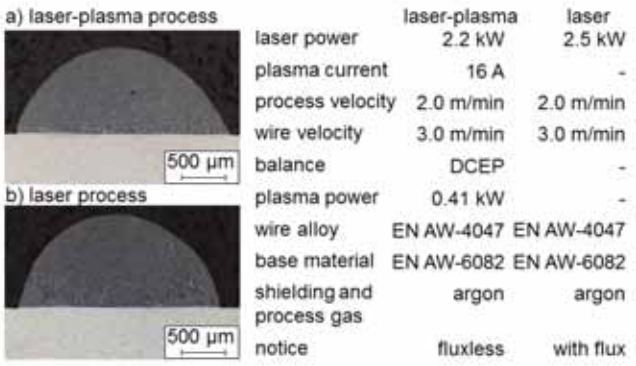

Fig. 3. Cross-sections of bead-on-plate seams brazed by different processes: (a) laser-plasma and (b) laser (BIAS ID 160082).

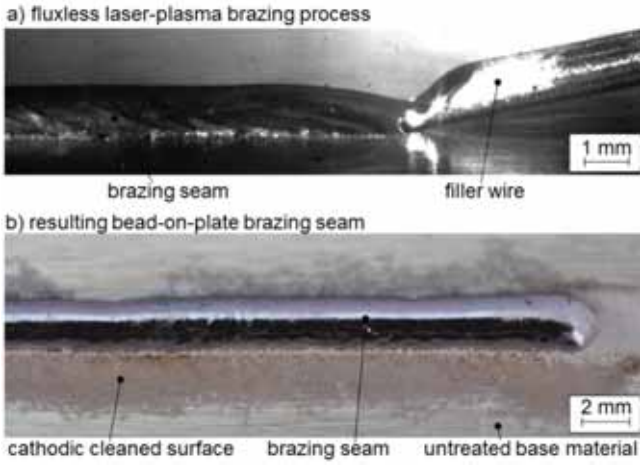

Fig. 4. (a) Fluxless laser-plasma brazing process and (b) the resulting bead-on-plate seam
(BIAS ID 160083).

4 Simulation of aluminum brazing

4.1 Geometry and mesh

For simulation purposes, a CAD geometry of the specimen dimensions (length of 150 mm, width of 50 mm and thickness of 2 mm) has been created. The model has been subdivided into three sections along the length axis, at 70 mm and 80 mm, respectively, in order to allow the cutting of the component in the following. The bead-on-plate brazing occurs towards the length direction of the plate. The component has been meshed with linear 8-node hexahedral elements with typical edge lengths of 1 mm in the component plane. The mesh has been refined in a distance of 5 mm from the weld line, reaching 0.25 mm element edge length in the middle section, **Fig. 2**. In the depth direction an element edge length of 0.5 mm has been used for the complete model.
Overall, approx. 130.000 elements have been used. The geometry of the filler material, i.e. of the seams in case of bead-on-plate, has been created based on

metallographic cross-sections and modeled accordingly with approx. 5500 (solely laser based process) and 8500 (laser-plasma process) hexahedral elements with a 0.5 mm characteristic edge length, respectively. The cross-sections of used fillets are shown, **Fig. 5**. The filler is mechanically activated in the simulation by a threshold temperature using the quiet element method. Such elements have negligible low stiffness values until the liquidus temperature is achieved.

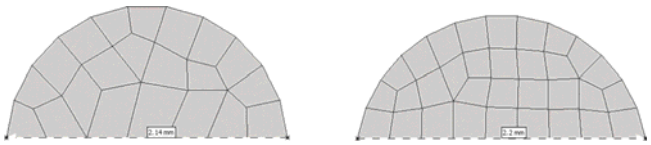

Fig. 5. Cross-sections of filler material seams: laser process (left, 1 mm high) and laser-plasma process (right, 0.925 mm high).

4.2 Heat Sources

4.2.1 Laser heat source

The heat source definition is based on measurements of the laser source and matchings to metallographic cross-sections. The heat source has been modeled using constant heat flux distribution over the depth and the radius of the heat source geometry with an effective heat source radius of 1.3 mm. The diameter of the laser heat source has been slightly reduced compared to measurements because the non-constant heat flux distribution of a laser was neglected.
Like the experimental setup, the heat source is mainly positioned on the filler material with some minor heat inputs on its left and right side. We considered the heat flux being applied to the volume of the model only, neglecting the surface portion. Due to convex shape of the surface only elements in the middle of the cross-section would experience any surface heat flux otherwise.
The output power of the laser source was 2500 W in the experiments. For the simulation we considered an efficiency factor of 0.4.

4.2.2 Combined laser-plasma heat source

Table 1. Heat source parameters.

Process type	**Laser**	**Hybrid**	
Shape	Cylindrical	Cylindrical	Goldak
Distribution	Constant	Constant	Gaussian
Depth mm	1.3	1.3	1.2
Width mm	1.3	1.3	1.5
Front length mm	-	-	2
Rear length mm	-	-	4
Power W	2500	2200	400
Efficiency	0.4	0.4	0.4

The combined heat source is represented by two heat fluxes distributed over the predefined heat source volume. A cylindrical heat source analogous to the aforementioned one with a laser output power of 2200 W has been combined with a plasma heat source in form of a Goldak double-ellipsoid geometry [13] with 400 W overall power. The exact parameters are listed, **Table 1**. The brazing velocity lies at 2 m/min for both processes.

4.3 Material model

Temperature dependent material properties of the EN AW-6082 aluminum alloy (AlSi1MgMn) have been provided by the Simufact.material database. The material has been modeled with respect to transformation enthalpy during melting and solidification which leads to heat transfer equation [14].

$$\rho C_p \frac{\partial T}{\partial t} - q - H - \nabla \cdot (\lambda \nabla T) = 0$$

The temperature dependent behavior of the filler material EN AW-4047 (AlSi12) has been calculated using JMatPro material simulation software based on alloying element composition. Stress-strain-relations have been added by scaling existing material data with respect to material specifications [15].
A completely melting of the filler material without any melting of the base material sheet is possible due to the lower melting temperature of the EN AW-4047 alloy (liquidus and solidus temperature being 590 °C and 570 °C, respectively) compared to the EN AW-6082 alloy (653 °C and 647 °C, respectively). Both temperatures have been calculated with JMatPro release 8.0, a material simulation software by Sente Software Ltd., and differ slightly from published material specifications.
The material data for both materials includes temperature-dependent properties for thermal expansion, Young's modulus, specific heat capacity, thermal conductivity and stress-strain-relations. Poisson's ratio has been considered constant over the whole temperature range. Strain rate dependencies of flow curves have been neglected.

4.4 Boundary conditions

As mechanical boundary conditions, a bearing underneath the component, gravity perpendicular to the bearing surface and friction forces between the component and bearings have been applied. Thus, stability of the model is assured and rigid body motion after unclamping is prohibited. Additionally, a clamp is applied along the x-axis of the model, **Fig. 2**. The stiffness is set to 10 kN/m and a force of 1 kN prevents rigid body motion during brazing, which can occur due to high forces present in the model while heating and cooling are applied. An overview over the mentioned conditions and their positions within a cross-section of the model is given, **Fig. 6**.
Thermal boundary conditions are represented by radiation according to Stefan-Boltzmann's law and free

convection with a convective heat transfer coefficient h of 20 W/(m²K) and an emissivity ε of 0.6.

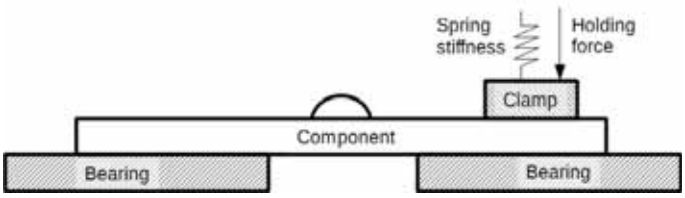

Fig. 6. Applied mechanical boundary conditions within a cross-section of the model.

4.5 Cutting

In the experiments, the component is cut after cooling. This step is represented in the model by removing the elements of the middle 10 mm wide strip, **Fig. 2**.

4.6 Simulation timetable

The brazing process takes 3.6 s. Afterwards a free cooling is applied. The clamp in the model is removed when the peak temperature falls below 20.1 °C for the first time (approx. 180 s after the process begin). The aforementioned cutting procedure is executed by removing the strip elements including the according part of the seam after 300 s. Afterwards, several time steps are considered in order to reach approximately equilibrium state. The calculation is finished after 600 s, **Fig. 7**.

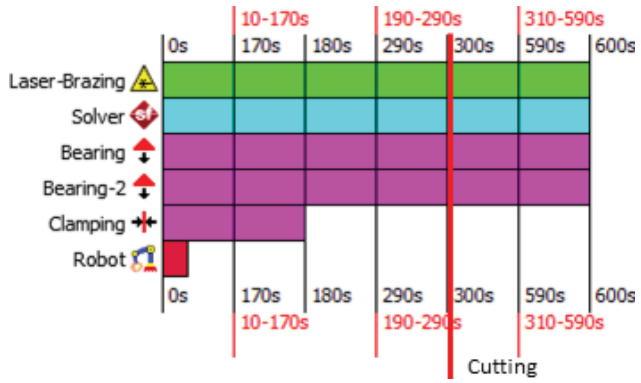

Fig. 7. Simulation steps over time. Laser-Brazing and Solver stand for the overall calculation period, while Robot represents the brazing process itself. Also, activation times of boundary conditions are visible.

4.7 Solution procedure

The solution has been obtained by a fully coupled thermo-mechanical calculation. Within the increments, a solution for the temperature field is found by means of the backward difference method. The material data is adjusted according to the local temperature. The resulting thermal strains representing mechanical loading of the model are calculated by structural analysis steps.
Within the contact interface between filler material and component a “bonded” joint is established by setting the contact condition to glue after achieving the liquidus temperature during the brazing simulation. Deformations of the seam, i.e. of the “bonded” filler material, due to shrinkage affect the shape of the component. The shrinkage, being asymmetrical to the central plane of the base sheet, leads to a bending, so-called angular distortion, in the direction of the heat source after cooling.

5 Model sensitivity

A structural simulation has to be calibrated in order to achieve the best possible results. There is a number of sensitive parameters whose influences on the results of the simulation depend on a process under investigation as well as solution and modeling method. For this study, the following sensitive parameters have been identified. In order to calculate a proper temperature field (which leads to better approximation of thermal strains as well as resulting material properties) especially the shape, the geometry and the efficiency of the heat source are important parameters. Both should be derived from temperature measurements and cross-section micrographs if available. However, a variation of these parameters within a range being typical for such a process causes a maximum change of the bending angle of 10 %. The maximum impact on the result seems to be provided by the flow stress data of the filler material.
Several model parameters have solely numerical character and are difficult to calibrate, e.g. the separation stress threshold which determines the critical stress when two surfaces (for example the bearing representing a table and the component) are separated in the simulation. Fortunately, this parameter has no significant influence on the result data in this study, **Table 2**.

Table 2. Model parameters and its influences on the results (- -: no influence, ++: high influence).

Input	**Output sensitivity**	
Parameter	Temperature field	Bending angle
Heat source geometry	++	+
Heat source efficiency	++	+
Clamping conditions	-	+
Separation stress threshold	- -	-
Thermal expansion coefficient	- -	+
Flow curves data	- -	++

Parameters which are marked with “+” change the result in comparison with the uncalibrated value by approx. 10 %, if the variation lies in a reasonable range. The results show maximum sensitivity with respect to the yield stress of the materials. Even changes within the material specification affect the bending angle by over 200 %.

6 Simulation results

The calibration of the heat input is usually crucial for a structural simulation as it determines the temperature field and the mechanical response of the model. In Simufact.welding, it is possible to reduce influences of overestimated temperature by deactivating further thermal expansion after the threshold of the melting temperature. Furthermore, other relevant material parameters can be “frozen”, i.e. fixed at the current values, when the solidus temperature is achieved. Nonetheless, two main goals are considered in terms of the calibration of the temperature field: the filler material has to be completely melted while the base material may achieve its melting temperature only in the upper element layer.

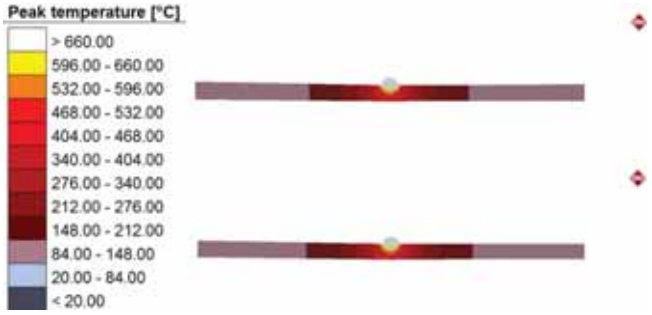

Fig. 8. Peak temperatures during the simulations of the solely laser (top) and the hybrid laser-plasma brazing process (bottom).

The peak temperatures in both simulations (with and without an additional plasma heat source) are similar due to only slight differences in the applied effective power values (1000 W in the laser vs. 1040 W in the combined laser-plasma process) as can be seen in the cross-sections of the model, **Fig. 8**.
The bending angles have been measured for evaluation of the quality of the mechanical model. The experimental results yield bending angles between 1.0° and 1.5° with the mean value and standard deviation of 1.29° ± 0.17° for the laser process as well as between 0.99° and 1.36° with the mean value and standard deviation of 1.13° ± 0.12° for the combined laser-plasma-approach without flux agent, respectively.
The simulations show bending angles of 1.10° for the laser process and 1.00° for the laser-plasma process. Both simulation results lie at the lower end of the measured range, just 0.02° and 0.01°, respectively, outside of the confidence interval. The results imply that a minor adaption of the heat source geometry or efficiency would further improve the match between experiments and simulations according to the angular distortion. However, it has to be remarked that the determined differences between experimental and numerical results are actually low for a basically uncalibrated model.
An advantage of a structural simulation of brazing and welding processes lies in the possibility of obtaining information about residual stresses as well as material behavior (e.g. hardening), which is usually only available by expensive and time-consuming experimental measurements. If predicted distortions are comparable to the associated experimental data, the simulation results for residual stresses and hardening are in general trustful. It has to be noted that the influence of the cutting process itself (i.e. the generated heat and mechanical effects on the material by a cutting tool) are neglected in this study. Nonetheless, the evaluated stresses in some distance to the cutting edge provide realistic information.
Comparing the states of the equivalent stress field before (**Fig. 9 left**) and after unclamping (**Fig. 9 center**) as well as after cutting (**Fig. 9 right**) shows that the unclamping step leads to a minor stress relief around the heat source path, while the cutting step seems to release stresses in the middle of the remaining components. However, the stress situations around the start and the end of the seam remain unaffected as they are enough far away from the cut. Some new stresses are induced around the cutting edge.

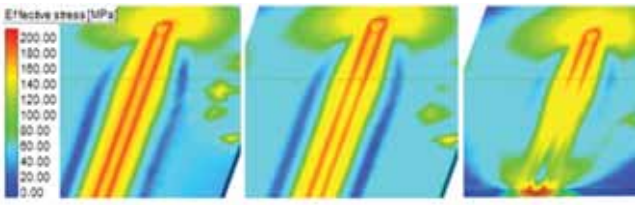

Fig. 9. Residual stress field during the simulation of the laser-plasma process: before (left) and after (center) unclamping as well as after cutting (right, cutting edge in front of the figure). The dotted line shows the measurement line represented in the following diagrams.

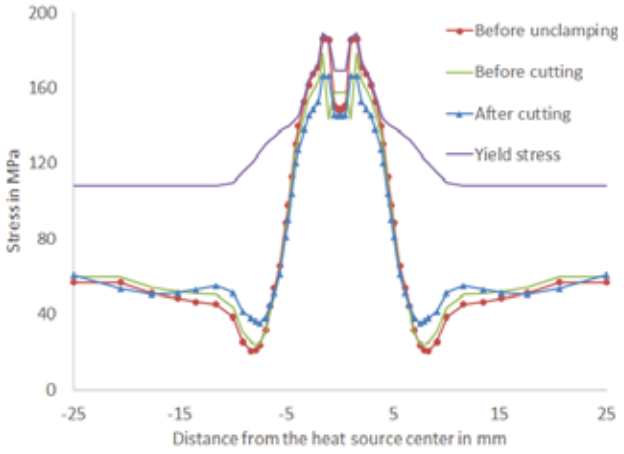

Fig. 10. Equivalent stresses before unclamping, before and after cutting as well as the resulting yield stress are shown in case of the laser process.

The residual stresses as well as the resulting yield stress depend on plastic strains and hardening effects of the material. The behaviors are shown for the laser brazing and for the laser-plasma brazing process, **Fig. 10** and **Fig. 11**, respectively. The dotted line illustrates the measurement line, **Fig. 9**. Yield stress is not influenced by unclamping and cutting of the component.

From the simulation point of view, the outcome of the experimental work, namely the general applicability of a hybrid laser-plasma brazing process without flux agents for aluminum welding as well as the tendency to lower distortion, is proven by the simulations. The calculated residual stresses for both process variants are almost similar with equal peak values, but slightly different distributions.

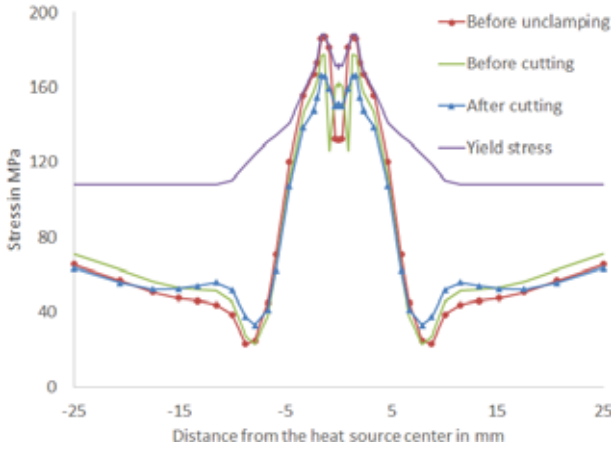

Fig. 11. Equivalent stresses before unclamping, before and after cutting as well as the resulting yield stress are shown in case of the laser-plasma process.

7 Summary

Experiments demonstrate the applicability of a hybrid laser-plasma process setup for fluxless aluminum welding. Although the wetting length in case of the hybrid process design is longer, i.e. increased seam width, the angular distortion tends to be lower. Thus, the production steps of applying, drying and removal of the flux agent could be eliminated offering the potential to decrease costs.
The simulations have shown that the technology being state-of-the-art for structural welding simulation is also well-suitable for brazing processes. The result quality seems to depend mainly on available material data, especially on temperature dependent flow stress data of used filler material, having high impact on the bending angle. It has been demonstrated that FE-simulation can predict, on the one hand, distortions. The distortion behavior can be easily compared with experimental results and used for validating and calibrating of the simulation model. Afterwards, the simulation can be applied, on the other hand, for calculation of hardly obtainable values like residual stresses and material hardenings.

Acknowledgements

Part of this work was accomplished within the Center of Competence for Welding of Aluminium Alloys – CentrAl. Funding by the Deutsche Forschungsgemeinschaft DFG (VO 530/44-2) is gratefully acknowledged.

References

[1] Hornig, H.: Praxis des Laserstrahlhartlötens im Fahrzeugbau. 5. Laser-Anwenderforum, eds.: Vollertsen, F.; Seefeld, T. BIAS-Verlag (2006), pp. 123 - 137
[2] Markovits, T.; Takács, J.; Lovas, A.; Belt, J.: Laser brazing of aluminium. Journal of Materials Processing Technology 143-144 (2003), pp. 651-655
[3] Braumöller, J.: Beitrag zum flussmittelfreien Laserstrahlhartlöten von Aluminiumwerkstoffen. Diss., Technische Universität Dresden. 2003
[4] Donst, D., Janssen, A., Niessen, M., Klocke, F.: Laser pulse influence on spreading of AlSi12-solder during fluxless laser brazing of aluminum, in Proc. of ICALEO 2009, pp. 440-448
[5] Goecke S. F., Wilden J., Jahn S., Reich S., Fedtke A., Vollertsen F., Thomy C.: Technologiekette zum Produzieren, Reparieren und Recyceln von Produkten in Material-Mix-Bauweise – PROREMIX. In: DVS-Berichte Band 250, DVS-Verlag, Düsseldorf (2008) pp. 75 - 78
[6] Klocke, F., Castell-Codesal, A., & Senster, P. (2003). Laserstrahlhartlöten von Aluminium. Wt Werkstattstechnik Online, 93(6), pp. 447 - 451
[7] Herbst, H. T.: Characteristics of the Arc in "Heliarc" Welding. Electrical Engineering (1948), pp. 30 - 33
[8] Stute, U.; Kling, R.; Hermsdorf, J.: Interaction between Electrical Arc and Nd: YAG Laser Radiation, CIRP Annals - Manufacturing Technology, 56, 1, (2007), pp. 197 - 200
http://dx.doi.org/10.1016/j.cirp.2007.05.048.
[9] Casalino, G., Campanelli, S.L., Dal Maso, U., Ludovico, A.D.: Arc leading versus laser leading in the hybrid welding of aluminium alloy using a fiber laser. In: Procedia CIRP 12 (2013), pp. 151 - 156
[10] Rippl, P: Anwendungsbeispiele für die Laser-Hybrid-Technik konventionell und mit Lasern geringer Leistung. In. 6. Strahltechnik Band 36. Laseranwenderforum (LAF'08), eds.: F. Vollertsen, T. Seefeld. BIAS-Verlag, pp. 107 – 117
[11] Schumacher, A., Hierold, R., Binde, P.: Finite-Element-Berechnung am Konstruktionsarbeitsplatz – Konzept und Realisierung. Konstruktion (2002) 11/12. pp. 71-76
[12] Sekulić, P: Modeling of the sequence of phenomena in brazing, in: Advances in brazing – Science, technology and applications, Eds.: D. P. Sekulić, Woodhead Publishing (2013), pp. 55 ff.
[13] Goldak, J.; Chakravarti, A.; Bibby, M.: A new finite element model for welding heat sources. In Metallurgical Trans. B, Vol. 15, Iss. 2 (1984), pp. 299 - 305
[14] Qin, G.; Su, Y.; Meng, X. and B. Fu: Numerical simulation on MIG arc brazing-fusion welding of aluminum alloy to galvanized steel plate. In Int. J. Adv. Manuf. Technol. 78 (2015), pp. 1917 - 1925
[15] EWM Handbuch Schweißzusatzwerkstoffe, 4. Auflage (2014)